

A Curriculum Domain Adaptation Approach to Semantic Segmentation of Urban Scenes

Yang Zhang¹, Philip David², Hassan Foroosh,¹ and Boqing Gong³

¹ University of Central Florida

² Computational and Information Sciences Directorate, U.S. Army Research Laboratory

³ Tencent A.I.

yangzhang@knights.ucf.edu, philip.j.david4.civ@mail.mil, foroosh@cs.ucf.edu,
boqinggo@outlook.com

Abstract—

During the last half decade, convolutional neural networks (CNNs) have triumphed over semantic segmentation, which is one of the core tasks in many applications such as autonomous driving. However, to train CNNs requires a considerable amount of data, which is difficult to collect and laborious to annotate. Recent advances in computer graphics make it possible to train CNNs on photo-realistic synthetic imagery with computer-generated annotations. Despite this, the domain mismatch between the real images and the synthetic data cripples the models' performance. Hence, we propose a curriculum-style learning approach to minimize the domain gap in urban scenery semantic segmentation. The curriculum domain adaptation solves easy tasks first to infer necessary properties about the target domain; in particular, the first task is to learn global label distributions over images and local distributions over landmark superpixels. These are easy to estimate because images of urban scenes have strong idiosyncrasies (e.g., the size and spatial relations of buildings, streets, cars, etc.). We then train a segmentation network while regularizing its predictions in the target domain to follow those inferred properties. In experiments, our method outperforms the baselines on two datasets and two backbone networks. We also report extensive ablation studies about our approach.

1 INTRODUCTION

SEMANTIC segmentation is one of the most challenging and fundamental problems in computer vision. It assigns a semantic label to each pixel of an input image [1]. The resulting output is a dense and rich annotation of the image, a semantic label per pixel. Semantic segmentation facilitates many downstream applications, including autonomous driving, which, over the past few years, has made great strides towards use by the general population. Indeed, several datasets and test suites have been developed for research on autonomous driving [2], [3], [4], [5], [6] and, among them, semantic segmentation is often considered one of the key tasks.

Convolutional neural networks (CNNs) [7], [8] have become a hallmark backbone model to solve the semantic segmentation of large-scale image sets over the last half decade. All the top-performing methods on the challenge board of the Cityscapes pixel-level semantic labeling task [2] rely on CNNs. One of the reasons that CNNs are able to achieve a high level of accuracy for this task is that the training set is sufficiently large and well-labeled, covering the variability of the test set for the research purpose. In practice, however, it is often hard to acquire new training sets that fully cover the huge variability of real-life test scenarios. Even if one can compose a large-scale dataset with sufficient variability, it is extremely tedious to label the images with pixel-wise semantic labels. For example, Cordts et al. report that the annotation and quality control took more than 1.5 hours per image in the popular Cityscapes dataset [2].

These challenges motivate researchers to approach the segmentation problem by using complementary synthetic data. With decent graphics engines, automatically synthesizing diverse urban-scene images along with pixel-wise labels would require very little to zero human interference. Figure 3 shows some synthetic images of the GTA dataset [6]. They are quite photo-realistic, giving rise to the hope that a semantic segmentation neural network trained from them can perform reasonably well on the real images too. However, our experiments show that it is not the case (cf. Section 4) at all, signifying a severe mismatch between the real images and the synthesized ones. Multiple factors may contribute to the mismatch, such as the capture device (camera vs. rendering engine), view angles, lighting condition and shadows, textures, etc.

In this paper, our main objective is to investigate the use of domain adaptation techniques [9], [10], [11], [12] to more effectively transfer the semantic segmentation neural networks trained using synthetic images to segmentation networks for real images. We build our efforts upon our prior work [11], in which we propose a novel domain adaptation approach to the semantic segmentation of urban scenes.

Domain adaption, which mainly aims to boost models' performance when the target domain of interest differs from the one where the models are trained, has long been a popular topic in machine learning and computer vision [13]. It has recently drawn even greater attention along with transfer learning thanks to the prevalence of deep neural networks which are often "data-hungry." An intuitive domain adaptation strategy is to learn domain-invariant feature representations for the images of both domains,

where the source domain supplies a labeled training set and the target domain reveals zero to a few labeled images along with many unlabeled ones. In this case, the source domain features would resemble the target ones’ characteristics. Thus, the model trained on the labeled source domain can be generalized to the target domain. Earlier “shallow” methods achieve such goals by exploiting various intrinsic structures of the data [14], [15], [16], [17], [18], [19], [20], [21]. In contrast, the recent “deep” methods mainly devise new loss functions and/or network architectures to add domain-invariant ingredients to the gradients backpropagating the neural networks [22], [23], [24], [25], [26].

Upon observing the success of learning domain-invariant features, it is a natural tendency to follow the same principle for the domain adaptation of semantic segmentation models. There have been some positive results along this line [10], [12]. However, the underlying assumption of this principle may prevent the methods designed around it from achieving high adaptation performance. By focusing on learning domain-invariant features X (i.e., such that $P_S(X) \approx P_T(X)$, where the subscripts S and T stand for the source and target domains, respectively), one assumes the conditional distribution $P(Y|X)$, where Y are the pixel labels, is more or less shared by the two domains. This assumption is less likely true when the classification boundary becomes more and more sophisticated — the prediction function for semantic segmentation has to be sophisticated. The sets of pixel labels are high-dimensional, highly structured, and interdependent, implying that the learner has to resolve the predictions in an exponentially large label space. Besides, some discriminative cues in the data would be suppressed if one matches the feature representations of the two domains without taking careful account of the structured labels. Finally, data instances are the proxy to measure the domain difference [25], [26], [27]. However, it is not immediately clear what comprises the instance in semantic segmentation [10], especially given that the top-performing segmentation methods are built upon deep neural networks [7], [28], [29], [30]. Hoffman et al. take each spatial unit in the fully convolutional network (FCN) [7] as an instance [10]. We contend that such instances are actually non-i.i.d. in either individual domain, as their receptive fields overlap with each other.

How can we avoid the assumption that the source and target domains share the same prediction function in a transformed domain-invariant feature space? Our proposed solution draws on two key observations. One is that urban traffic scene images have strong idiosyncrasies (e.g., the size and spatial relations of buildings, streets, cars, etc.). Therefore, some tasks are “easy” and, *more importantly, suffer less because of the domain discrepancy*. Second, the structured output in semantic segmentation enables convenient posterior regularization [31], as opposed to the popular (e.g., ℓ_2) regularization over model parameters.

Accordingly, we propose a curriculum-style [32] domain adaptation approach. Recall that, in domain adaptation, only the source domain supplies many labeled data while there are no or only scarce labels from the target domain. The curriculum domain adaptation begins with the easy tasks, in order to gain some high-level properties about the unknown pixel-level labels for each target image. It then learns a semantic segmentation network, the hard task, whose predictions over the target images are constrained to follow those necessary properties as much as possible.

To develop the easy tasks for the curriculum, we consider estimating label distributions over both global images and some landmark superpixels of the target domain. Take the former, for

instance. The label distribution indicates the percentage of pixels in an image that correspond to each category. We argue that these tasks are easier, despite the domain mismatch, than assigning pixel-level labels. The label distributions are only rough estimations about the labels. Moreover, the size relations between road, building, sky, people, etc. constrain the shape of the distributions, effectively reducing the search space for learning models. Finally, models to estimate the label distributions over superpixels may benefit from the urban scenes’ canonical layout that transcends domains, e.g., buildings stand beside streets.

Why and when are these seemingly simple label distributions useful for the domain adaptation of semantic segmentation? In our experiments, we find that the segmentation networks trained on the source domain perform poorly on many target images, giving rise to disproportionate label assignments (e.g., many more pixels are classified to sidewalks than to streets). To rectify this, the image-level label distribution informs the segmentation network *how* to update the predictions while the label distributions of the anchor superpixels tell the network *where* to update. Jointly, they guide the adaptation of the networks to the target domain to, at least, generate proportional label predictions. Note that additional “easy tasks” can be incorporated into our approach in the future.

Our main contribution is the proposed curriculum-style domain adaptation for the semantic segmentation of urban scenes. We select for the curriculum the easy and useful tasks of inferring label distributions for both target images and landmark superpixels in order to gain some necessary properties about the target domain. Built upon these, we learn a pixel-wise discriminative segmentation network from the labeled source data and, meanwhile, conduct a “sanity check” to ensure the network behavior is consistent with the previously learned knowledge about the target domain. Our approach effectively eludes the assumption about the existence of a common prediction function for both domains in a transformed feature space. It readily applies to different segmentation networks as it does not change the network architecture nor impact any intermediate layers.

Beyond our prior work [11], we provide more details and experimental studies about our approach, including new experiments using the GTA dataset [6], ablation study about the number of superpixels, various backbone neural networks, prediction confusion matrix etc. In addition, we introduce a color constancy scheme into our framework. It significantly improves the adaptation performance and may be plugged into any domain adaptation method as a standalone image pre-processing step. Finally, we also quantitatively measure the “market value” of the synthetic data.

2 RELATED WORK

We discuss related work on domain adaptation and semantic segmentation, with special focus on transferring knowledge from synthetic to real images.

2.1 Domain adaptation

Conventional machine learning algorithms rely on the assumption that the training and test data are drawn i.i.d. from the same underlying distribution. However, it is often the case that there exists some discrepancy between the training and test stages. Domain adaptation aims to rectify this mismatch and tune the models toward better generalization at testing [27], [33], [34], [35], [36].

The existing work on domain adaptation mostly focuses on classification and regression problems [37], [38], e.g., learning from online images to classify real world objects [14], [39], and, more recently, aims to improve the adaptability of deep neural networks [23], [24], [25], [26], [40]. Among them, the most relevant works to ours are those exploring simulated data [10], [41], [42], [43], [44], [45], [46]. Sun and Saenko train generic object detectors from synthetic images [41], while Vazquez et al. use virtual images to improve pedestrian detections in real environments [44]. The other way around, i.e., how to improve the quality of the simulated images using the real ones, is studied in [45], [46].

2.2 Semantic segmentation

Semantic segmentation is the task of assigning an object label to each pixel of an image. Traditional methods [47], [48], [49] rely on local image features manually designed by domain experts. After the pioneering works [7], [30] that introduced the convolutional neural network (CNN) [50] to semantic segmentation, most recent top-performing methods are built on CNNs [29], [51], [52], [53], [54], [55].

Currently, there are multiple and increasing numbers of semantic segmentation datasets aiming for different computer vision applications. Some general ones include the PASCAL VOC2012 Challenge [56] which contains nearly 10,000 annotated images for the segmentation competition, and the MS COCO Challenge [57] which includes over 200,000 annotated images. In our paper, we focus on urban outdoor scenes. Several urban scene segmentation datasets are publicly available including CityScapes [2], a vehicle dashcam dataset created primarily in German cities; KITTI [58], another vehicle-centric dataset captured in the German city Karlsruhe; Berkeley DeepDrive Video Dataset [3], a dashcam dataset collected in United States; Mapillary Vistas Dataset [59], so far known as the largest outdoor urban scene segmentation dataset collected from all over the world; WildDash, a much smaller yet equivalently diverse dataset for benchmark purpose only; and CamVid [60], a small, low-resolution toy dashcam dataset. An enormous amount of labor-intensive work is required to annotate the many images that are needed to obtain accurate segmentation models. According to [6], it took about 60 minutes to manually segment each image in [61] and about 90 minutes for each in [2]. A plausible approach to reducing the human annotation workload is to utilize weakly supervised information such as image labels and bounding boxes [28], [62], [63], [64].

We instead explore the almost labor-free labeled virtual images for training high-quality segmentation networks. In [6], annotating a synthetic image took only 7 seconds on average through a computer game. For the urban scenes, we use the SYNTHIA [43] and GTA [6] datasets which contain images of virtual cities. Although not used in our experiments, another synthetic segmentation dataset worth mentioning is Virtual KITTI [65], a synthetic exact duplication of the original aforementioned KITTI [66] road scene dataset.

2.3 Domain adaptation for semantic segmentation

Upon observing the obvious mismatch between virtual and real data [6], [43], [67], we expect domain adaptation to enhance the segmentation performance on real images by networks trained on virtual ones. To the best of our knowledge, the first attempt to algorithmically address this problem before ours is [10]. The

problem itself subsequently became one of the tracks in the Visual Domain Adaptation Challenge (VisDA) 2017 [12] and is receiving increasing attention. After that, other feature-alignment based methods [9], [68], [69], [70], [71] emerged. The reader should note that the winning solutions in VisDA are very heavily engineered ensemble models containing several state-of-art complicated segmentation networks. Most of the aforementioned works were inspired by the unsupervised adversarial domain adaptation approach of [72], which is similar in approach to the generative adversarial neural network. Their training objective is to generate a homogeneous intermediate feature distribution by attempting to deceive a domain classifier. Meanwhile, we propose a different curriculum domain adaptation strategy [11]. We solve the easy task first and then use the learned knowledge about the target domain to regularize the network predictions.

A well-adapted semantic segmentation model will subsequently benefit other closely related, higher-level applications that are trained and deployed in different environments. Such applications include autonomous driving systems trained in the AirSim [4] or CARLA [5] synthetic autonomous driving environments, and indoor robotic agents trained in the interactive AI2THOR [73] environment.

3 APPROACH

In this section, we present the details of our approach to curriculum domain adaptation for semantic segmentation of urban scene images. Unlike previous works [10], [37] that align the domains via an intermediate feature space and thereby implicitly assume the existence of a single decision function for the two domains, it is our intuition that, for structured prediction (i.e., semantic segmentation here), the cross-domain generalization of machine learning models can be more efficiently improved if we avoid this assumption and instead train them subject to necessary properties they should retain in the target domain. After a brief introduction on the preliminaries, we will present how to facilitate semantic segmentation adaptation during training using estimated target domain properties in the Section 3.2. Then we will focus on the type of target domain properties and how to estimate them in the Section 3.3.

3.1 Preliminaries

In particular, properties of interest concern pixel-wise category labels $Y_t \in \mathbb{R}^{W \times H \times C}$ of an arbitrary image $I_t \in \mathbb{R}^{W \times H}$ from the target domain, where W and H are the width and height of the image, respectively, and C is the number of categories. We use one-hot vector encoding for the groundtruth labels, i.e., $Y_t(i, j, c)$ takes the value of either 0 or 1, where the latter means that the c -th label is assigned by a human annotator to the pixel at (i, j) . Correspondingly, the prediction $\hat{Y}_t(i, j, c) \in [0, 1]$ by a segmentation network is realized by a softmax function per pixel.

We express each target property in the form of a distribution p_t over the C categories, where $\sum_c^C p_t(c) = 1$ and $0 \leq p_t(c), \forall c$. $p_t(c)$ represents the occupancy proportion of the category c over the t -th target image or a superpixel of that image. Therefore, one can immediately calculate the distribution p_t given the human annotations Y_t to the image. For instance, the image-level label distribution is expressed by

$$p_t(c) = \frac{1}{WH} \sum_{i=1}^W \sum_{j=1}^H Y_t(i, j, c), \quad \forall c. \quad (1)$$

Similarly, we can compute the estimated target property/distribution from the network predictions \widehat{Y}_t and denote it by \widehat{p}_t ,

$$\widehat{p}_t(c) = \frac{1}{WH} \sum_{i=1}^W \sum_{j=1}^H \left(\frac{\widehat{Y}_t(i, j, c)}{\max_{c'}(\widehat{Y}_t(i, j, c'))} \right)^K, \quad \forall c \quad (2)$$

where $K > 1$ is a large constant whose effect is to “sharpen” the softmax activation per pixel $\widehat{Y}(i, j, c)$ such that the summand is either 1 or very close to 0, in a similar shape as the summand $Y_t(i, j, c)$ of eq. (1). We set $K = 6$ in our experiment as larger K caused numerical instability. Finally, we ℓ_1 -normalize the vector $(\widehat{p}(1), \widehat{p}(2), \dots, \widehat{p}(C))^T$ such that its elements are all greater than 0 and sum up to 1 — in other words, the vector remains a valid distribution.

3.2 Domain adaptation observing the target properties

Ideally, we would like to have a segmentation network imitate human annotators of the target domain. Therefore, necessarily, the properties of their annotation results should be the same too. We capture this notion by minimizing the cross entropy $\mathcal{C}(p_t, \widehat{p}_t) = H(p_t) + \text{KL}(p_t, \widehat{p}_t)$ at training, where the first term of the right-hand side is the entropy and the second is the KL-divergence.

Given a mini-batch consisting of both source images (S) and target images (T), the overall objective function for training the cross-domain generalizing segmentation network is

$$\min \frac{\gamma}{|S|} \sum_{s \in S} \mathcal{L}(Y_s, \widehat{Y}_s) + \frac{1-\gamma}{|T|} \sum_{t \in T} \sum_k \mathcal{C}(p_t^k, \widehat{p}_t^k) \quad (3)$$

where \mathcal{L} is the pixel-wise cross-entropy loss defined over the sufficiently labeled source domain images, enforcing the network to have the pixel level discriminative capabilities, and the second term is over the unlabeled target domain images, hinting the network what necessary properties its predictions should have in the target domain. We use $\gamma \in [0, 1]$ to balance the two strengths in training and superscript k to index different types of label distributions (cf. p_t in eq. (1) and Section 3.3).

Note that, in the unsupervised domain adaptation context, we actually cannot directly compute the label distributions $\{p_t^k\}$ because the groundtruth annotations of the target domain are unknown. Nonetheless, using the labeled source domain data, these distributions are easier to estimate than are the labels for every pixel of a target image. We present two types of such properties and the details for inferring them in the next section. In future work, it is worth exploring other properties.

Remarks. Mathematically, the objective function has a similar form as model compression [74], [75]. Hence, we borrow some concepts to gain a more intuitive understanding of our domain adaptation procedure. The “student” network follows a curriculum to learn simple knowledge about the target domain before it addresses the hard one of semantically segmenting images. The models inferring the target properties act like “teachers”, as they hint what label distributions the final solution (image annotation) may have in the target domain at the image and superpixel levels.

Another perspective is to understand the target properties as a posterior regularization [31] for the network. The posterior regularization can conveniently encode a priori knowledge into the objective function. Some applications using this approach include weakly supervised segmentation [28], [52] and detection [76], and rule-regularized training of neural networks [77]. In addition to the

domain adaptation setting and novel target properties, another key distinction of our work is that we decouple the label distributions from the network predictions and thus avoid the EM type of optimization, which is often involved and incurs extra computational overhead. Our approach learns the segmentation network with almost effortless changes to the popular deep learning tools.

3.3 Inferring the target properties

Thus far, we have presented the “hard” task — learning the segmentation neural network — in the curriculum domain adaptation. In this section, we describe the “easy” tasks, i.e., how to infer the target domain properties without any annotations from the target domain. Our contributions also include selecting the particular property of label distributions to constitute the simple tasks.

3.3.1 Global label distributions over images

Due to the domain disparity, a baseline segmentation network trained on the source domain (i.e., using the first term of eq. (3)) could be easily crippled given the target images. In our experiments, we find that our baseline network constantly mistakes streets for sidewalks and/or cars (cf. Figure 3). Consequently, the predicted labels for the pixels are highly disproportionate.

To rectify this, we employ the label distribution p_t over the global image as our first property (cf. eq. (1)). Without access to the target labels, we have to train machine learning models from the labeled source images to estimate the label distribution p_t of a target image. Nonetheless, we argue that this is less challenging than generating per-pixel predictions despite that both tasks are influenced by the domain mismatch.

In our experiments, we examine several different approaches to this task. We extract 1536D image features from the output of last average pooling layer in Inception-Resnet-v2 [78] as the input to the following models.

Logistic regression. Although multinomial logistic regression (LR) is mainly used for classification, its output is actually a valid distribution over the categories. For our purpose, we thus train it by replacing the one-hot vectors in the cross-entropy loss with the groundtruth label distribution p_s , which is counted by using eq. (1) from the human labels of the source domain. Given a target image, we directly take the LR’s output as the estimated label distribution p_t .

Mean of nearest neighbors. We also test a nonparametric method by simply retrieving multiple nearest neighbor (NN) source images for each target image and then transferring the mean of the source’s label distributions to the target image. We use the ℓ_2 distance in the Inception-Resnet-v2 feature space for the NN retrieval.

Finally, we include two dumb predictions as the control experiments. One is, for any target image, to output the mean of all the label distributions in the source domain (**source mean**), and the other is to output a **uniform distribution**.

3.3.2 Local label distributions of landmark superpixels

The image-level label distribution globally penalizes potentially disproportional segmentation output in the target domain, and yet is inadequate in providing spatial regularization to the network. In this section, we consider the use of label distributions over some superpixels as the anchors to drive the network towards spatially desired target properties.

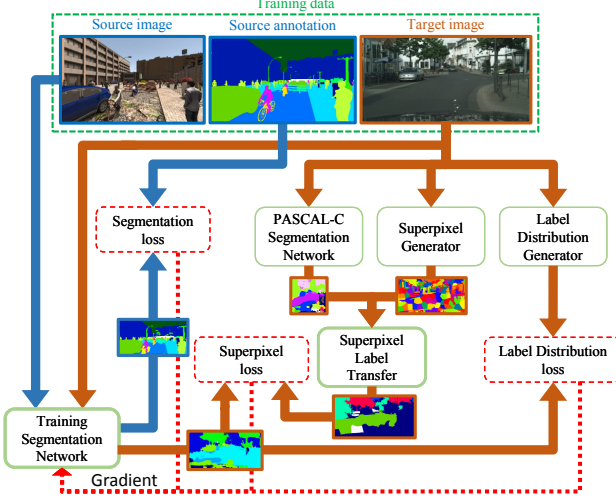


Fig. 1: The overall framework of our curriculum domain adaptation approach for the semantic segmentation of urban scenes.

Note that it is not necessary, and is even harmful, to use all of the superpixels in a target image to regularize the segmentation network because it would be too strong a force and might overrule the pixel-wise discriminativeness (obtained from the fully labeled source domain), especially when the label distributions are not inferred accurately enough.

In order to have the dual effect of both estimating the label distributions of some superpixels and selecting them from all candidate superpixels, we employ a linear SVM in this work. We first segment each image into 100 superpixels using linear spectral clustering [79]. For the superpixels of the source domain, we are able to assign a single dominant label to each of them and then train a multi-class SVM using the “labeled” superpixels of the source domain. Given a test superpixel of a target image, the multi-class SVM returns a class label as well as a decision value, which is interpreted as the confidence score about classifying this superpixel. We keep the top 30% most confident superpixels in the target domain. The class labels are then encoded into one-hot vectors which serve as valid distributions about the category labels upon the selected landmark superpixels’ area. Albeit simple, we find this method works very well.

In order to train the aforementioned superpixel SVM, we need to find a generalized way to represent the superpixels in a feature space. We encode both visual and contextual information to represent a superpixel. First, we use the FCN-8s [7] pre-trained on the PASCAL CONTEXT [80] dataset, which has 59 distinct classes, to obtain 59 detection scores for each pixel. We then average these scores within each superpixel. The final feature representation of a superpixel is a 295D concatenation of the 59D vectors of itself, its left and right superpixels, as well as the two respectively above and below it.

3.4 Curriculum domain adaptation: recapitulation

We recap the proposed curriculum domain adaptation using Figure 1 before presenting the experiments in the next section. Our main idea is to execute the domain adaptation step by step, starting from the easy tasks that, compared to semantic segmentation, are less sensitive to domain discrepancy. We choose the labels distributions over global images and local landmark superpixels in this work; more tasks will be explored in the future. The

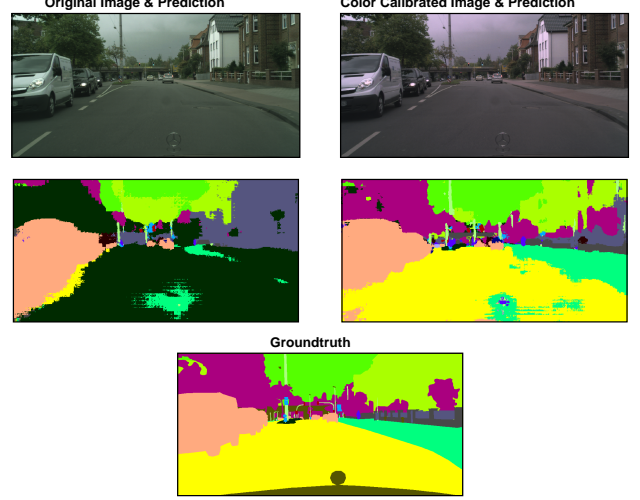


Fig. 2: Predictions of the same FCN-8s model, without domain adaptation, before and after altering the image’s color.

solutions to them provide useful gradients originating from the target domain (cf. the arrows with brown color in Figure 1), while the source domain feeds the network with well-labeled images and segmentation masks (cf. the dark blue arrows in Figure 1).

3.5 Color Constancy

In this subsection, we propose an color calibration preprocessing step which we find very effective in adapting semantic segmentation methods from the synthetic to the real image domains. We assume color of target domain images and source domain images are drawn from different distribution. And such difference has a substantial impact on the segmentation network performance. Thus calibrating target images’ color to the source ones would improve the performance. We describe it independently of the main body of our approach summarized in Section 3.4 because it can stand alone and can be added to any existing method for domain adaptation models.

Humans have the ability to perceive the same color of an object even when it is exposed in different illuminations [81], but image capturing sensors do not, in general. As a result, different illuminations result in different RGB images captured by the cameras. Subsequently, perception incoherence limits the performance of computer vision algorithms [82] because the illumination is often among the key factors that cause the domain mismatch. To this end, we propose to use computational color constancy [83] to eliminate the influence of illuminations.

The goal of color constancy is to correct the colors of images acquired under unconventional or biased light sources to their colors under the reference lighting condition. In our domain adaptation scenario, we assume that the source domain resembles the reference lighting condition. We learn a parametric model to describe both of the target and source light sources and then try to restore the target images according to the source domain’s light source. However, not all the color constancy methods are applicable. For instance, some methods rely on physics priors or the statistics of natural images, both of which are unavailable in synthetic images.

Due to the above concerns, we instead use a gamut-based color constancy method [84] to align the target and source images in

terms of their colors. This method infers the property of the light source under the assumption that only a limited range of color could be observed under a certain light source. This matches our assumption that the target images' colors and the source images' colors belong to different distribution/range. In addition to the pixel values, the image edge and derivatives are also used to find the mapping. While we omit the details of this color constancy method and refer the readers to [84] instead, we show in Figure 2 how sensitive the segmentation model is to the illumination. We can see that, prior to applying color constancy, a large part of a CityScapes image is incorrectly classified as "terrain" only because the image is a little greenish.

4 EXPERIMENTS

In this section, we run extensive experiments to verify the effectiveness of our approach and study several variations of it to gain a thorough understanding about how different components contribute to the overall results. We investigate the global image-wise label distribution and the local landmark superpixels by separate experiments. We also empirically examine the effects of distinct granularities of the superpixels as well as different feature representations of the superpixels. Moreover, we compare our approach with several competing baselines for the adaptation of various deep neural networks from two synthetic datasets for the urban scene segmentation task. We use confusion matrices to show how different classes of the urban scene images intervene with each other. Finally, we run few-shot adaptation experiments by gradually revealing some labels of the images of the target domain. The results show that, even when more than 1,000 target images are labeled (50% of the Cityscapes training set [2]), the adaptation from synthetic images is still able to boost the results by a relatively large margin.

4.1 Segmentation network and optimization

In most of our experiments, we use FCN-8s [7] as our semantic segmentation network. We initialize its convolutional layers with VGG-19 [85] and then train it using the AdaDelta optimizer [86] with default parameters. Each mini-batch is comprised of five source images and five randomly chosen target images. When we train the baseline network with no adaptation, however, we try to use the largest possible mini-batch which includes 15 source images. The network is implemented in Keras [87] and Theano [88]. We train different versions of the network on a single Tesla K40 GPU.

There is an ablation experiment using the state-of-the-art segmentation neural network ADEMXAPP [89]. The training details and architecture are described in Section 4.7.

We note that our curriculum domain adaptation can be readily applied to other segmentation networks (e.g., [29], [30]). Once we infer the label distributions of the unlabeled target images and some of their landmark superpixels, we can use them to train different segmentation networks by eq. (3) without changing them.

4.2 Datasets and evaluation

We use the publicly available **Cityscapes** [2] as our target domain in the experiments. For the source domains of synthesized images, we test both **GTA** [6] and **SYNTHIA** [43].

Cityscapes is a real-world vehicle-egocentric image dataset collected from 50 cities in Germany and the countries around

It provides four disjoint subsets: 2,993 training images, 503 validation image, 1,531 test images, and 20,021 auxiliary images. All the training, validation, and test images are accurately annotated with per-pixel category labels, while the auxiliary set is coarsely labeled. There are 34 distinct categories in the dataset. Among them, 19 categories are officially recommended for training and evaluation.

SYNTHIA [43] is a large dataset of synthetic images and provides a particular subset, called **SYNTHIA-RAND-CITYSCAPES**, to pair with Cityscapes. This subset contains 9,400 images that are automatically annotated with 12 object categories, one void class, and some unnamed classes. Note that the virtual city used to generate the synthetic images does not correspond to any of the real cities covered by Cityscapes.

GTA [6] is a synthetic vehicle-egocentric image dataset collected from the open world in the realistically rendered computer game, Grand Theft Auto V (GTA). It contains 24,996 images. Unlike the **SYNTHIA** dataset, its semantic segmentation annotation is fully compatible with the Cityscapes dataset. Hence, we will use all the 19 official training classes in our experiment.

4.2.1 Domain idiosyncrasies

Although all datasets depict urban scenes and both **SYNTHIA** and **GTA** are created to be as photo-realistic as possible, they are mismatched domains in several ways. The most noticeable difference is probably the coarse-grained textures in **SYNTHIA**; very similar texture patterns repeat in a regular manner across different images. The textures in **GTA** are better but still visibly artificial. In contrast, the **Cityscapes** images are captured by high-quality dash-cameras. Another major distinction is the variability in view angles. Since **Cityscapes** images are recorded by the dash cameras mounted on a moving car, they are viewed from almost a constant angle that is about parallel to the ground. More diverse view angles are employed by **SYNTHIA** — it seems like some cameras are placed on the buildings that are significantly higher than a bus. Most **GTA** images are dashcam images, but some of them are captured from the view points of the pedestrians. In addition, some of the **SYNTHIA** images are severely shadowed by extreme lighting conditions, while we find no such conditions in the **Cityscapes** images. Finally, there is a subtle difference in color between the synthetic images and the real ones due to the graphics rendering engines' systematic performance. For instance, the **GTA** images are overly saturated (cf. Figure 3) and **SYNTHIA** images are overly bright in general. These combined factors, among others, make domain adaptation from **SYNTHIA** and **GTA** to **Cityscapes** a very challenging problem.

Figure 3 show some example images from the three datasets. We pair each **Cityscapes** image with its nearest neighbor in **GTA**, retrieved by the Inception-Resnet-v2 [78] features. However, many of the cross-dataset nearest neighbors are visually very different from the query images, verifying the dramatic disparity between the two domains.

4.2.2 Evaluation

We use the evaluation code released along with the **Cityscapes** dataset to evaluate our results. It calculates the PASCAL VOC intersection-over-union, i.e., $\text{IoU} = \frac{\text{TP}}{\text{TP} + \text{FP} + \text{FN}}$ [56], where TP , FP , and FN are the numbers of true positive, false positive, and false negative pixels, respectively, determined over the whole test set. Since we have to resize the images before feeding them to the segmentation network, we resize the output segmentation mask

7
 Fig. 3: Qualitative semantic segmentation results on the Cityscapes dataset [43] (target domain). For each target image in the first column, we retrieve its nearest neighbor from the
 GTA [6] dataset (source domain). The third column plots the label distributions due to the groundtruth pixel-wise semantic annotation, the predictions by the baseline network with no
 adaptation, and the inferred distribution by logistic regression. The last three columns are the segmentation results by the baseline network, our domain adaptation approach, and human
 annotators, respectively.

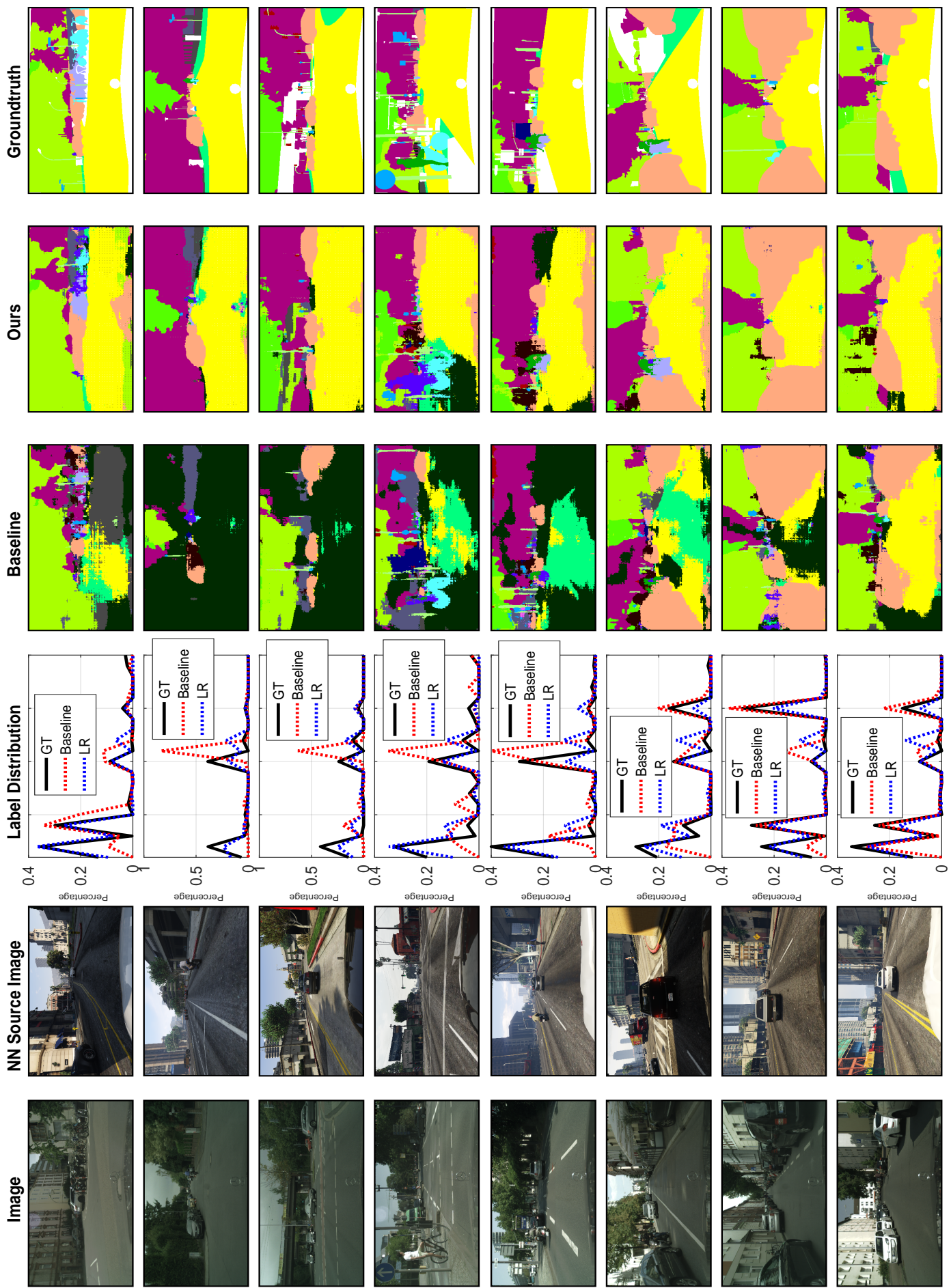


TABLE 1: χ^2 distances between the groundtruth label distributions and those predicted by different methods for the adaptation from SYNTHIA to Cityscapes.

Method	Uniform	NoAdapt	Src mean	NN	LR
χ^2 Distance	1.13	0.65	0.44	0.33	0.27

back to the original image size before running the evaluation against the groundtruth annotations.

4.3 Results of inferring global label distribution

Before presenting the final semantic segmentation results, we first compare different approaches to inferring the global label distributions over the target images (cf. Section 3.3.1). We use SYNTHIA and Cityscapes’ held-out validation images as the source domain and the target domain, respectively, in this experiment.

In Table 1, we compare the estimated label distributions with the groundtruth ones using the χ^2 distance, the smaller the better. We see that the baseline network (NoAdapt), which is directly learned from the source domain without any adaptation methods, outperforms the dumb uniform distribution (Uniform) and yet no other methods. This confirms that the baseline network gives rise to severely disproportional predictions on the target domain.

Another dumb prediction (Src mean), i.e., using the mean of all label distributions over the source domain as the prediction for any target image, however, performs reasonably well. This is mainly because the protocol layouts of the urban scene images. To some extent, the results implies that the images from the simulation environments share at least similar layouts as the real images, indicating the value of the simulated source domains for the semantic segmentation task of urban scenes.

Finally, the nearest neighbor (NN) based method and the multinomial logistic regression (LR) (cf. Section 3.3.1) perform the best. We use the output of LR on the target domain in our remaining experiments.

4.4 Domain adaptation experiments

In this section, we present our main results of this paper, i.e., comparison results for the domain adaptation from simulation to real images for the semantic segmentation task. Here we focus on the base segmentation neural network FCN-8s [7]. Another network, ADEMXAPP [89], is studied in Section 4.7.

Since our ultimate goal is to solve the semantic segmentation problem for the real images of urban scenes, we take Cityscapes as the target domain and SYNTHIA/GTA as the source domain. We split 500 images out of the Cityscapes training set for the validation purpose (e.g., to monitor the convergence of the networks). In training, we randomly sample mini-matches from both the images and labels of SYNTHIA/GTA and the remaining images of Cityscapes yet with no labels. The Cityscapes validation set is used as our test set.

All the 19 classes provided by GTA are used in the experiments. For the adaptation from SYNTHIA to Cityscapes, we manually find 16 common classes between the two datasets: sky, building, road, sidewalk, fence, vegetation, pole, car, traffic sign, person, bicycle, motorcycle, traffic light, bus, wall, and rider. The last four are unnamed and yet labeled in SYNTHIA.

4.4.1 Baselines

We compare our approach to the following competing methods.

No adaptation (NoAdapt). We directly train the FCN-8s model on SYNTHIA without applying any domain adaptation methods. This is the most basic baseline for our experiments.

Superpixel classification (SP). Recall that we have trained a multi-class SVM using the dominant labels of the superpixels in the source domain. We then use it to classify the target superpixels.

Landmark superpixels (SP Lndmk). Since we keep the top 30% most confidently classified superpixels as the landmarks to regularize our segmentation network during training (cf. Section 3.3.2), it is also interesting to examine the classification results of these superpixels. We execute the evaluation after assigning the void class label to the other pixels of the images. In addition to the IoU, we have also evaluated the classification results of the superpixels by accuracy for the domain adaptation experiments from SYNTHIA and Cityscapes. We find that the classification accuracy is 71% for all the superpixels of the target domain. For the top 30% landmark superpixels, the classification accuracy is more than 88%.

FCNs in the wild (FCN Wild). Hoffman et al.’s work [10] was the only existing one addressing the same problem as ours when we published the conference version [11] of this work, to the best of our knowledge. They introduce a pixel-level adversarial loss to the intermediate layers of the network and impose constraints to the network output. Their experimental setup is about identical to ours except that they do not specify which part of Cityscapes is considered as the test set. Nonetheless, we include their results for comparison to put our work in a better perspective.

4.4.2 Comparison results

The comparison results of adapting from SYNTHIA to CityScapes are shown in Table 2. We also present the results of adapting from GTA to CityScapes in Table 3. Immediately, we note that all our domain adaptation results are significantly better than those without adaptation (NoAdapt) in both tables.

We denote by **(Ours (I))** the network regularized by the global label distributions over the target images. Although one may wonder that the image-wise label distributions are too abstract to supervise the pixel-wise discriminative network, the gain is actually significant. They are able to correct some obvious errors of the baseline network, such as the disproportional predictions about road and sidewalk (cf. the results of **Ours (I)** vs. NoAdapt in the last two columns of Tables 2 and 3).

It is interesting to see that both superpixel classification-based segmentation results (SP and SP Lndmk) are also better than the baseline network (NoAdapt). The label distributions obtained over the landmark superpixels boost the segmentation network **(Ours (SP))** to the mean IoU of 28.1% and 27.8% respectively when adapting from SYNTHIA and Cityscapes, which are better than those by either superpixel classification or the baseline network individually. We have also tried to use the label distributions over all the superpixels to train the network, and observe little improvement. This is probably because it is too forceful to regularize the network output at every single superpixel especially when the estimated label distributions are not accurate enough.

The superpixel-based methods, including **Ours (SP)**, miss small objects, such as pole and traffic signs (t-sign), and instead

TABLE 2: Comparison results for adapting the FCN-8s model from SYNTHIA to Cityscapes.

Method	%	IoU	SYNTHIA2CityScape Class-wise IoU															
			bike	fence	wall	t-sign	pole	mbike	t-light	sky	bus	rider	veg	bldg	car	person	sidewalk	road
NoAdapt [10]		17.4	0.0	0.0	1.2	7.2	15.1	0.1	0.0	66.8	3.9	1.5	30.3	29.7	47.3	51.1	17.7	6.4
FCN Wld [10]		20.2	0.6	0.0	4.4	11.7	20.3	0.2	0.1	68.7	3.2	3.8	42.3	30.8	54.0	51.2	19.6	11.5
NoAdapt		22.0	18.0	0.5	0.8	5.3	21.5	0.5	8.0	75.6	4.5	9.0	72.4	59.6	23.6	35.1	11.2	5.6
NoAdapt (CC)		22.6	22.2	0.5	1.1	5.0	21.5	0.6	8.5	73.4	4.8	9.2	73.2	56.7	28.4	34.8	12.1	9.1
Ours (I)		25.5	16.7	0.8	2.3	6.4	21.7	1.0	9.9	59.6	12.1	7.9	70.2	67.5	32.0	29.3	18.1	51.9
Ours (CC+I)		27.3	31.2	1.3	3.9	6.0	19.4	2.1	9.2	61.2	11.2	7.4	68.3	65.1	41.4	29.3	18.9	60.6
SP Lndmk (CC)		23.1	0.0	0.0	0.0	0.0	0.0	0.0	0.0	82.6	27.8	0.0	73.1	67.9	40.7	5.8	10.3	62.2
SP (CC)		25.6	0.0	0.0	0.0	0.0	0.0	0.0	0.0	80.1	22.7	0.0	72.2	69.7	45.6	25.0	19.4	74.8
Ours (SP)		28.1	10.2	0.4	0.1	2.7	8.1	0.8	3.7	68.7	21.4	7.9	75.5	74.6	42.9	47.3	23.9	61.8
Ours (CC+SP)		28.9	17.7	0.5	0.5	3.4	10.9	1.8	5.4	73.4	17.6	9.9	76.8	74.5	43.7	44.4	22.4	59.6
Ours (I+SP)		29.0	13.1	0.5	0.1	3.0	10.7	0.7	3.7	70.6	20.7	8.2	76.1	74.9	43.2	47.1	26.1	65.2
Ours (CC+I+SP)		29.7	20.3	0.6	0.5	4.3	14.0	1.9	5.3	73.7	21.2	11.0	77.8	74.7	44.8	45.0	23.1	57.4

TABLE 3: Comparison results for adapting the FCN-8s model from GTA to Cityscapes.

Method	%	IoU	GTA2CityScape Class-wise IoU																		
			bike	fence	wall	t-sign	pole	mbike	t-light	sky	bus	rider	veg	terrain	train	bldg	car	person	truck	sidewalk	road
NoAdapt [10]		21.1	0.0	3.1	7.4	1.0	16.0	0.0	10.4	58.9	3.7	1.0	76.5	13	0.0	47.7	67.1	36	9.5	18.9	31.9
FCN Wld [10]		27.1	0.0	5.4	14.9	2.7	10.9	3.5	14.2	64.6	7.3	4.2	79.2	21.3	0.0	62.1	70.4	44.1	8.0	32.4	70.4
NoAdapt		22.3	13.8	8.7	7.3	16.8	21.0	4.3	14.9	64.4	5.0	17.5	45.9	2.4	6.9	64.1	55.3	41.6	8.4	6.8	18.1
NoAdapt (CC)		26.2	16.2	10.9	8.8	18.5	23.3	7.0	13.2	62.7	5.4	19.0	65.1	5.8	2.3	64.8	63.9	42.2	9.2	13.8	45.0
Ours (I)		23.1	9.5	9.4	10.2	14.0	20.2	3.8	13.6	63.8	3.4	10.6	56.9	2.8	10.9	69.7	60.5	31.8	10.9	10.8	26.4
Ours (CC+I)		28.5	7.2	9.4	11.1	13.4	23.1	9.6	15.1	64.6	5.9	15.5	71.1	10.3	3.9	67.7	62.3	43.0	14.0	23.0	71.6
SP Lndmk (CC)		21.6	0.0	0.0	0.0	0.0	0.0	0.0	0.0	82.4	9.1	0.0	74.4	22.2	0.0	70.3	53.1	15.3	11.2	6.9	65.8
SP (CC)		26.8	0.3	2.3	6.8	0.0	0.2	3.4	0.0	80.5	25.5	4.1	73.5	31.4	0.0	71.0	61.6	28.2	30.4	17.3	73.3
Ours (SP)		27.8	15.6	11.7	5.7	12.0	9.2	12.9	15.5	64.9	15.5	9.1	74.6	11.1	0.0	70.5	56.1	34.8	15.9	21.8	72.1
Ours (CC+SP)		30.2	10.4	13.6	10.3	14.0	13.9	18.8	16.5	73.6	14.1	9.5	79.2	12.9	0.0	74.3	63.5	33.1	18.9	27.5	70.5
Ours (I+SP)		28.9	14.6	11.9	6.0	11.1	8.4	16.8	16.3	66.5	18.9	9.3	75.7	13.3	0.0	71.7	55.2	38.0	18.8	22.0	74.9
Ours (CC+I+SP)		31.4	12.0	13.2	12.1	14.1	15.3	19.3	16.8	75.5	19.0	10.0	79.3	14.5	0.0	74.9	62.1	35.7	20.6	30.0	72.9

are very accurate for categories like the sky, road, and building, which typically occupy larger image regions. On the contrary, the label distributions on the images give rise to a network (**Ours (I)**) that performs better on the small objects than **Ours (SP)**. In other words, they mutually complement to some extent. Retraining the network by using the label distributions over both global images and local landmark superpixels (**Ours (I+SP)**), we achieve semantic segmentation results on the target domain that are superior over using either to regularize the network.

Finally, we report the results of our method and its ablated versions (i.e., **Ours (I+SP)** **Ours (I)** and **Ours (SP)**) after we apply color constancy to the images (accordingly, the methods are denoted by **Ours (CC+I+SP)**, **Ours (CC+I)**, and **Ours (CC+SP)**). We observe improvements of various degrees over those before the color constancy. Especially, the best results are obtained after we apply the color constancy for adapting from both SYNTHIA and Cityscapes.

4.4.2.1 Comparison with FCNs in the wild [10]: Although we use the same segmentation network (FCN-8s) as [10], our baseline results (NoAdapt) are better than those reported in [10]. This may be due to subtle differences in terms of implementation or experimental setup. In either case, we gain larger improvements (7.7%/9%) over the baseline [10].

4.4.2.2 Comparison with learning domain-invariant features: At our first attempt to solve the domain adaptation problem for the semantic segmentation of urban scenes, we tried to learn domain invariant features following the deep domain adaptation methods [23] for classification. In particular, we impose the maximum mean discrepancy [90] over the layer before the output. We

name such network layer the feature layer. Since there are virtually three output layers in FCN-8s, we experiment with all the three feature layers correspondingly. We have also tested the domain adaptation by reversing the gradients of a domain classifier [26]. However, none of these efforts lead to any noticeable gain over the baseline network so the results are omitted.

4.4.3 Confusion between classes

While Tables 2 and 3 show the overall and per-class results, they do not tell the confusion between different classes. In this section, we provide the confusion matrices of some methods in order to provide more informative analyses about the results. Considering the page limit, we present the confusion matrices of NoAdapt and **Ours (CC+I+SP)** for the adaptations from SYNTHIA and GTA to CityScapes by Figure 4.

We find that a lot of objects are misclassified to the “building” category, especially the classes “pole”, “traffic sign”, “traffic light”, “fence” and “wall”. It is probably because those classes often show up beside buildings and they all have huge intra-class variability. Moreover, the “pole”, “traffic sign”, and others are very small objects comparing to the “building”. Some special care is required to disentangle these classes from the “building” in the future work.

Another noticeable confusion is between the “train” and the “bus”. After analyzing the data, we find that this is likely due to the lack of discrimination between the two classes by the datasets themselves, rather than the algorithms. In Figure 4, we visualize some trains and buses in the GTA dataset and some trains in the Cityscapes dataset. The difference between the trains and the buses

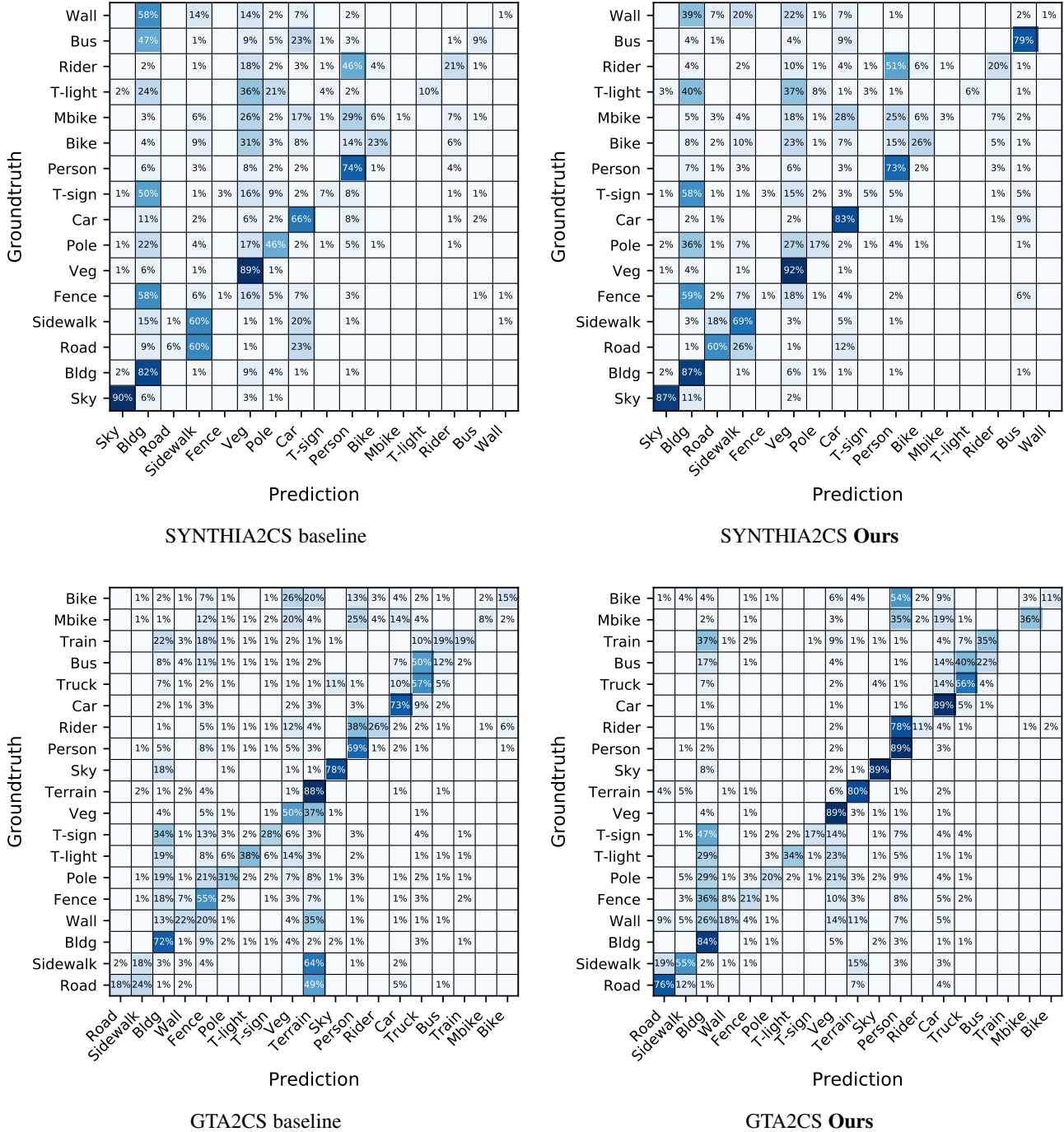


Fig. 4: Confusion matrices for the baseline of no adaptation (left) and **Ours (CC+I+SP)** (right) for the experiments of SYNTHIA-to-CityScape (SYNTHIA2CS, top) and GTA-to-CityScapes (GTA2CS, bottom).

turns out very subtle. We could make mistakes too if we do not pay attention to the rails (e.g., the train on the bottom right could be easily misclassified as a bus). Probably this confusion between trains and buses could be alleviated if more training examples can be supplied.

4.5 Handcrafted features

We study whether the network is able to work under target properties derived from handcrafted features in this section. Recall that we represent a superpixel/image by using a network pre-trained

on PASCAL CONTEXT [80]/ImageNet. We are interested in examining whether such high-level semantic representations of the superpixels/images are necessary. Hence, we compare the high-level superpixel/image descriptors with the following descriptors.

BOW. We encode our superpixel with the bag-of-words (BOW)-SIFT features. We first extract dense SIFT features [91] from the input image and then encode those of each superpixel into a 100D BOW vector. The dictionary for the encoding is obtained by K-means clustering.

FV. We also include Fisher vectors (FV) [92], [93] to encode

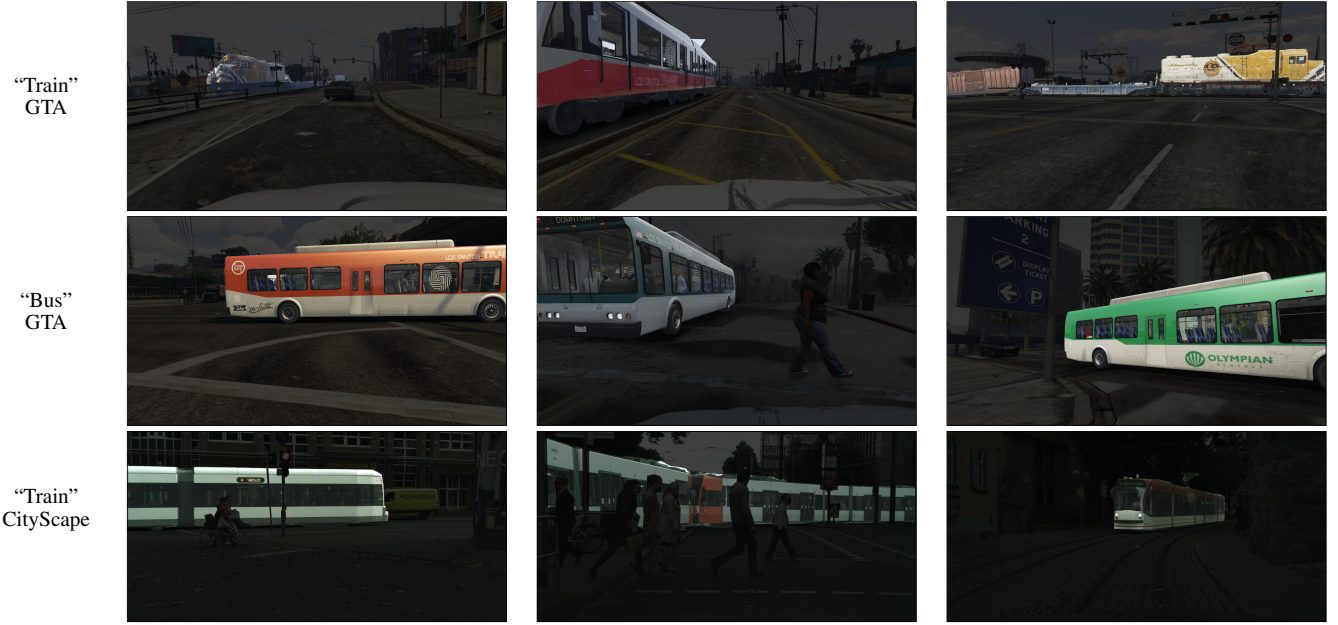


TABLE 4: Some “train” and “bus” images from the Cityscapes and GTA datasets. We can see that the CityScape “trains” are more visually similar to the GTA “buses” instead of the GTA “trains”.

TABLE 5: Results for the adaptation of FCN-8s from GTA to Cityscapes when we use handcrafted features instead of the CNN features.

Method	%	IoU	GTA2CityScape Class-wise IoU																			
			bike	fence	wall	t-sign	pole	mbike	t-light	sky	bus	rider	veg	terrain	train	bridge	car	person	truck	sidewalk	road	
NoAdapt (CC)		26.2	16.2	10.9	8.8	18.5	23.3	7.0	13.2	62.7	5.4	19.0	65.1	5.8	2.3	64.8	63.9	42.2	9.2	13.8	45.0	
Ours (CC+BOW)		27.9	13.8	14.0	9.6	17.9	23.9	6.4	16.7	64.6	3.0	18.0	69.1	7.0	2.4	69.2	60.1	44.0	10.7	19.1	60.8	
Ours (CC+FV)		28.1	13.3	10.5	12.8	18.6	24.4	5.1	10.8	63.5	1.7	14.6	73.5	10.0	0.3	71.6	66.6	40.8	6.1	11.5	79.0	
Ours (CC+BOW+FV)		28.3	15.3	13.3	11.6	18.5	25.1	6.7	16.8	66.5	2.9	18.4	72.2	8.7	2.6	70.0	59.4	43.9	10.8	19.1	56.8	

the SIFT features of each image into a fixed-dimension descriptor. We use a Gaussian mixture model with 8 Gaussian components. Each image is then represented by a 2048D vector. We train the dictionary for the bag-of-words and the Gaussian mixture model for the Fisher vectors using the SIFT features of the GTA dataset only.

Table 5 shows the results on adaptation from GTA to Cityscapes of our approach using the handcrafted two described above. We denote the resulting methods respectively by **Ours (CC+BOW)**, **Ours (CC+FV)**, and **Ours (CC+BOW+FV)** which use both label distribution and superpixel landmarks constraints built upon BOW and FV. It is interesting to see all of them outperform the baseline **NoAdapt (CC)**, indicating that our curriculum domain adaptation method is able to leverage the handcrafted features as well.

4.6 Granularity of the superpixels

In this section, we study what is a proper granularity of the superpixels. Intuitively, small superpixels are fine-grained and precisely tracks object boundaries. However, they are less discriminative as a result. What is a proper granularity of the superpixels? How sensitive could the results be to the granularity? To quantitatively answer these questions, we vary the number of superpixels per image to examine their effects on the semantic segmentation results. The adaptation from GTA of the **SP (CC)** method, described in Section 4.4.1, is reported in Table 6 with various numbers of

superpixels per image. In general, the performance increases as the number of superpixels grows until it reaches 300 per image.

Besides, we also presented the classification accuracy of the top $x\%$ superpixels in Figure 5, where $x = 0, 20, \dots, 100$. We can see that the accuracy is always more than 90% when we keep the top 20% or 40% superpixels per image — in our experiments, we keep top 30%. Besides, the accuracy of keep all the superpixels (top 100%) are not very high, indicating that it is not a good idea to use all superpixels to guide the training of the neural networks.

4.7 Domain adaptation experiments using ADEMXAPP

Our approach is agnostic to the base semantic segmentation neural networks. In this section, we further investigate a more recent network, ADEMXAPP [89], which is among the few top performing methods on the Cityscapes test set. Our experiment setup in this section resembles that of Section 4.4 except that we replace FCN-8s with the ADEMXAPP net. In particular, we reimplement the A1 model of ADEMXAPP using the Theano-Keras framework. However, we remove the batch normalization layers in our implementation due to their extensive GPU memory consumption. We follow the authors’ suggestions otherwise and initialize the network with the weights pre-trained on Imagenet. We set both the size of the mini-batch to be three for both the source domain and the target domain.

Table 7 shows the comparison results for the ADEMXAPP net. We can see it indeed achieves much better results than FCN-8s in

TABLE 6: Results for the adaptation of FCN-8s from GTA to Cityscapes when we use different numbers of superpixels per image. Here the images are pre-processed with color constancy.

SP # per image	IoU	GTA2CityScape Class-wise IoU																			
		bike	fence	wall	t-sign	pole	mbike	t-light	sky	bus	rider	veg	terrain	train	bldg	car	person	truck	sidewalk	road	
50	22.9	0.0	0.0	1.5	0.0	0.0	0.0	0.0	80.1	21.9	0.0	69.3	26.2	0.0	66.3	54.9	9.9	18.3	12.6	74.6	
100	26.8	0.3	2.3	6.8	0.0	0.2	3.4	0.0	80.5	25.5	4.1	73.5	31.4	0.0	71.0	61.6	28.2	30.4	17.3	73.3	
200	27.3	0.2	2.2	7.2	0.0	0.8	3.0	0.0	80.5	24.4	3.8	75.9	32.9	0.0	72.5	63.7	31.1	27.9	18.4	74.2	
400	27.4	0.4	3.8	7.2	0.0	1.1	1.7	0.0	80.7	23.2	3.7	76.9	33.3	0.0	72.5	63.8	33.1	26.9	18.4	73.3	

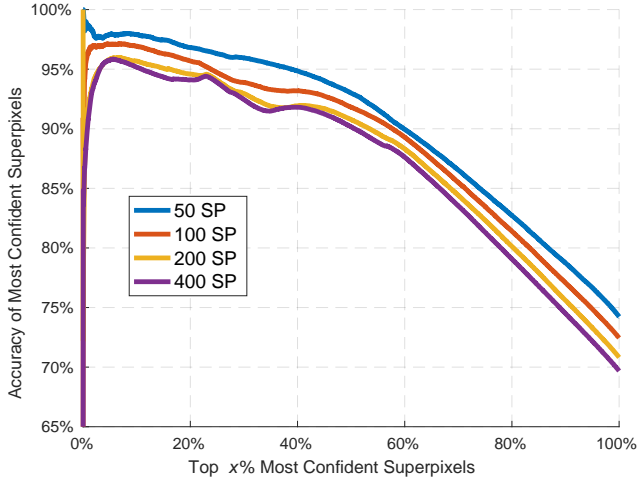


Fig. 5: We evaluate how many superpixels are accurate in the top $x\%$ confidently predicted superpixels. The experiments are conducted on the validation set of Cityscapes with color constancy.

general. Nonetheless, the observations about our approach remain the same for this ADEMAPP net.

4.8 What is the “market value” of the synthetic data?

Despite the positive results thus far for our curriculum domain adaptation from simulation to reality for the semantic segmentation of urban scenes, we argue that the significance of our work lies on its capability of complementing the training set of real data, rather than replacing it. In the long run, we expect that learning from both simulation and reality will alleviate the strong dependency of deep learning models on the massively labeled real training data. Therefore, it is interesting to evaluate the “market value” of the synthetic data: how many real training examples the GTA or SYNTHIA dataset can save in terms of the labeling efforts in order to achieve about the same level of segmentation accuracy?

In order to answer the above question, we design the following experiments. We gradually add some small portions of annotated CityScape images into the SYNTHIA training set. Every time doing this, we train two versions of the VGG-19-FCN-8s network respectively by using the enriched training set and the corresponding real images added to the training set. We use 2380 CityScape training images in the experiments since the remaining ones are reserved for the validation purpose.

Table 8 presents the results. First of all, it is somehow surprising to see that even as few as five CityScape training images added into the SYNTHIA training set can significantly boost the results obtained from the synthetic images only (33.8% vs. 22.0%). Second, the “N/A” results in the table mean that the corresponding

neural networks either give rise to random predictions or meet numerical issues. Note that such phenomena happen until there are more than 450 target images for the training without any synthetic images, implying that “market value” of the SYNTHIA training set is at least worth 450 well-labeled real images. Actually, if we compare the results of the two rows, the network trained from the mixed training set outperforms the one from the real images only up to the column of 50%. In other words, the SYNTHIA training set is able to help when the Cityscapes training set is smaller than 1000 images.

4.9 Comparison with more recent works

After we publish the main body of our work [11] on IEEE International Conference on Computer Vision in 2017, there have been notably a rich line of works tackling the same problem, i.e., domain adaptation for the semantic segmentation of urban scenes by adapting from the synthetic imagery to real images. Some of them have reported very good results. Since our approach is orthogonal in some sense to them, one may achieve better results by fusing our method with the existing ones. In this section, we give a brief review about them.

CyCADA [9]. The main idea is to transform the synthetic images of the source domain to the style of the target domain (real images) using CycleGAN [94] before feeding the source images to the segmentation network. Interestingly, CycleGAN and the segmentation network are trained simultaneously.

ROAD [70]. In the Reality Oriented Adaptation (ROAD) method [70], two losses are proposed to align the source and the target domain. The first one is called target guided distillation, which is a loss for regression from the segmentation network’s hidden layer activation of the source domain to the image features of the target domain. Here the image features are obtained by a classificaiton pre-trained on ImageNet. The other loss takes care of the spatial-aware adaptation. The features map of either a source image or a target image is partitioned into non-overlapping grids. After that, an maximum mean discrepancy loss [10] is introduced over each grid.

MCD [69]. The Maximum Classifier Discrepancy (MCD) resembles the recently popularized generative adversarial methods [72]. It learns two classifiers from the source domain and maximizes their disagreement on the target images in order to detect target examples that fall out of the support of the source domain. After that, it updates the generator to minimize the two classifiers’ disagreement on the target domain. By alternating the two steps in the training, it ensures that the generator gives rise to feature representations over which the source and the target domains are well aligned.

LSD [68]. This work is an adversarial domain adaptation network built upon an auto-encoder network. The network takes as

TABLE 7: Results for the adaptation of ADEMXAPP [89] from GTA to Cityscapes. The ADEMXAPP net is a more powerful semantic segmentation network than FCN-8s.

Method	%	IoU	GTA2CityScape Class-wise IoU																		
			bike	fence	wall	t-sign	pole	mbike	t-light	sky	bus	rider	veg	terrain	train	bldg	car	person	truck	sidewalk	road
FCN (CC)		26.2	16.2	10.9	8.8	18.5	23.3	7.0	13.2	62.7	5.4	19.0	65.1	5.8	2.3	64.8	63.9	42.2	9.2	13.8	45.0
ADEMXAPP (CC)		30.0	8.3	10.6	15.5	16.5	23.3	11.7	21.9	66.5	10.7	12.6	74.2	14.1	3.3	70.2	58.4	43.1	14.3	24.2	70.2
FCN (CC+SP)		30.2	10.4	13.6	10.3	14.0	13.9	18.8	16.5	73.6	14.1	9.5	79.2	12.9	0.0	74.3	63.5	33.1	18.9	27.5	70.5
ADEMXAPP (CC+SP)		34.0	8.8	12.4	18.4	15.3	22.5	16.6	18.5	73.7	24.5	10.9	76.7	22.9	0.1	74.3	72.3	40.3	21.3	32.9	83.1
FCN (CC+I)		28.5	7.2	9.4	11.1	13.4	23.1	9.6	15.1	64.6	5.9	15.5	71.1	10.3	3.9	67.7	62.3	43.0	14.0	23.0	71.6
ADEMXAPP (CC+I)		31.4	24.2	13.3	19.0	11.2	26.2	10.0	8.2	62.4	9.0	18.8	74.0	14.5	8.1	68.4	70.2	41.4	16.3	26.9	73.6
FCN (CC+I+SP)		31.4	12.0	13.2	12.1	14.1	15.3	19.3	16.8	75.5	19.0	10.0	79.3	14.5	0.0	74.9	62.1	35.7	20.6	30.0	72.9
ADEMXAPP (CC+I+SP)		35.7	9.6	13.6	21.9	14.2	25.0	15.7	19.2	72.3	22.1	18.1	77.7	19.7	14.5	77.8	73.3	46.4	17.4	33.8	85.0

TABLE 8: IoUs 1) after mixing different percentages of CityScape images into the SYNTHIA training dataset and 2) of models trained with different percentages of CityScape images with any SYNTHIA images.

CS images #	None	5 images	1%	2.5%	5%	10%	20%	50%	100%
SYN+CS	22.0%	33.8%	38.4%	41.0%	43.0%	46.5%	48.5%	53.2%	57.3%
CS only	N/A	N/A	N/A	N/A	N/A	N/A	38.4%	52.2%	57.8%

TABLE 9: Comparison with some recent works published after the conference version of our approach [11].

Method	Backbone Network	Adapt?	SYN2CS		GTA2CS	
			IoU	Gain	IoU	Gain
CyCADA	VGG16	Base	-	-	17.9	17.5
	FCN8s	Adapt	-	35.4		
	DRN26	Base	-	21.7		
	DRN26	Adapt	-	39.5	17.8	
ROAD	VGG16	Base	25.4		21.9	
	FCN8s	Adapt	36.2	10.8	35.9	13.0
MCD	VGG16	Base	-	-	24.9	3.9
	FCN8s	Adapt	-	-	28.8	
	DRN105	Base	23.4		22.2	
	DRN105	Adapt	37.3	13.9	39.7	17.5
LSD	VGG16	Base	26.8		29.6	
	FCN8s	Adapt	36.1	9.3	37.1	7.5
FCN Wld	Dialation Frontend	Base	17.4		21.1	
	Dialation Frontend	Adapt	20.2	2.8	27.1	6.0
Ours	VGG19	Base	22.0		22.3	
	FCN8s	Adapt	29.7	7.7	31.4	9.1
	ADEMXAPP	Base	-	-	30.0	
	ADEMXAPP	Adapt	-	-	35.7	5.7

input both source and target images and reconstructs them due to an auto-encoder loss. Meanwhile, an intermediate layer is connected to the segmentation network whose loss is defined using the labeled source images.

We summarize their reported results, along with ours and FCN Wld’s [10], in Table 9. Immediately, we can see that the backbone network has a huge impact on both the absolute performance and the relative gain of the performance, no matter with or without domain adaptation techniques. For example, the performance gain of MCD jumps from 3.9% to 17.5% after switching the backbone network from VGG to DRN [95].

Another interesting observation is that the results of no adaptation vary a lot even when the same backbone network (e.g., VGG16) is used, implying that small changes to the implementation (e.g., we have removed the batch normalization in order to save the computation cost) could lead to big difference in the final results. To some degree, this also indicates that, under the domain adaptation context, the neural networks becomes even more sensitive than they are for the conventional supervised learning problems.

Finally, we note that our approach is “orthogonal” to the re-

cently proposed methods because the curriculum training strategy can also be conveniently applied to them.

5 CONCLUSION

In this paper, we propose a curriculum domain adaptation approach to the semantic segmentation of urban scenes. We learn to estimate the global label distributions over the target images and local label distributions over the superpixels of the target images. These tasks are easier to solve than the pixel-wise label assignment. We then use their results to effectively regularize the training of the semantic segmentation networks such that their pixel-wise predictions are consistent with the global and local label distributions. We experimentally verify the effectiveness of our approach by adapting from the source domain of synthetic images to the target domain of real images. Our method outperforms several competing baselines. Moreover, we report several key ablation studies that allow us to gain more insights about the proposed method. We also check the class-wise confusion matrices and find that some of the classes (e.g., train and bus) are almost indistinguishable in the current datasets, indicating that better simulation or more labeled real examples are required in order to achieve better segmentation results. In the future work, we will explore more target properties that possess the same property as the global and local label distributions — they are easier to solve than the pixel-wise label prediction and meanwhile can be written as a function of the pixel-wise labels. We also would like to look into the possibility of directly applying our domain adaptation framework to virtual autonomous driving environments such as DeepGTAV [96] and AirSim [4].

ACKNOWLEDGMENTS

This work is supported by the NSF award IIS #1566511, a gift from Adobe Systems Inc., and a GPU from NVIDIA.

REFERENCES

- [1] A. Garcia-Garcia, S. Orts-Escolano, S. Oprea, V. Villena-Martinez, and J. Garcia-Rodriguez, “A review on deep learning techniques applied to semantic segmentation,” *arXiv preprint arXiv:1704.06857*, 2017.
- [2] M. Cordts, M. Omran, S. Ramos, T. Rehfeld, M. Enzweiler, R. Benenson, U. Franke, S. Roth, and B. Schiele, “The cityscapes dataset for semantic urban scene understanding,” in *Proceedings of the IEEE Conference on Computer Vision and Pattern Recognition*, 2016, pp. 3213–3223.

[3] H. Xu, Y. Gao, F. Yu, and T. Darrell, "End-to-end learning of driving models from large-scale video datasets," *arXiv preprint arXiv:1612.01079*, 2016.

[4] S. Shah, D. Dey, C. Lovett, and A. Kapoor, "Airsim: High-fidelity visual and physical simulation for autonomous vehicles," in *Field and Service Robotics*, 2017.

[5] A. Dosovitskiy, G. Ros, F. Codevilla, A. Lopez, and V. Koltun, "CARLA: An open urban driving simulator," in *Proceedings of the 1st Annual Conference on Robot Learning*, 2017, pp. 1–16.

[6] S. R. Richter, V. Vineet, S. Roth, and V. Koltun, "Playing for data: Ground truth from computer games," in *European Conference on Computer Vision*. Springer, 2016, pp. 102–118.

[7] J. Long, E. Shelhamer, and T. Darrell, "Fully convolutional networks for semantic segmentation," in *Proceedings of the IEEE Conference on Computer Vision and Pattern Recognition*, 2015, pp. 3431–3440.

[8] A. Krizhevsky, I. Sutskever, and G. E. Hinton, "Imagenet classification with deep convolutional neural networks," in *Advances in neural information processing systems*, 2012, pp. 1097–1105.

[9] J. Hoffman, E. Tzeng, T. Park, J.-Y. Zhu, P. Isola, K. Saenko, A. A. Efros, and T. Darrell, "Cycada: Cycle-consistent adversarial domain adaptation," *arXiv preprint arXiv:1711.03213*, 2017.

[10] J. Hoffman, D. Wang, F. Yu, and T. Darrell, "FCNs in the Wild: Pixel-level Adversarial and Constraint-based Adaptation," *arXiv preprint arXiv:1612.02649*, 2016.

[11] Y. Zhang, P. David, and B. Gong, "Curriculum domain adaptation for semantic segmentation of urban scenes," in *The IEEE International Conference on Computer Vision (ICCV)*, vol. 2, no. 5, Oct 2017, p. 6.

[12] X. Peng, B. Usman, N. Kaushik, J. Hoffman, D. Wang, and K. Saenko, "Visda: The visual domain adaptation challenge," *arXiv preprint arXiv:1710.06924*, 2017.

[13] G. Csurka, "Domain adaptation for visual applications: A comprehensive survey," *arXiv preprint arXiv:1702.05374*, 2017.

[14] B. Gong, Y. Shi, F. Sha, and K. Grauman, "Geodesic flow kernel for unsupervised domain adaptation," in *IEEE Conference on Computer Vision and Pattern Recognition (CVPR)*, 2012, pp. 2066–2073.

[15] R. Gopalan, R. Li, and R. Chellappa, "Domain adaptation for object recognition: An unsupervised approach," in *IEEE International Conference on Computer Vision (ICCV)*, 2011, pp. 999–1006.

[16] B. Fernando, A. Habrard, M. Sebban, and T. Tuytelaars, "Unsupervised visual domain adaptation using subspace alignment," in *IEEE International Conference on Computer Vision (ICCV)*, 2013, pp. 2960–2967.

[17] B. Sun, J. Feng, and K. Saenko, "Return of frustratingly easy domain adaptation," in *AAAI Conference on Artificial Intelligence (AAAI)*, 2016.

[18] S. J. Pan, J. T. Tsang, Ivor W. and Kwok, and Q. Yang, "Domain adaptation via transfer component analysis," *Transactions on Neural Networks*, vol. 22, no. 2, pp. 199 – 210, 2011.

[19] B. Gong, K. Grauman, and F. Sha, "Connecting the dots with landmarks: Discriminatively learning domain invariant features for unsupervised domain adaptation," in *International Conference on Machine Learning (ICML)*, 2013, pp. 222–230.

[20] R. Aljundi, R. Emonet, D. Muselet, and M. Sebban, "Landmarks-based kernelized subspace alignment for unsupervised domain adaptation," in *IEEE Conference on Computer Vision and Pattern Recognition (CVPR)*, 2015, pp. 56–63.

[21] B. Kulic, K. Saenko, and T. Darrell, "What you saw is not what you get: Domain adaptation using asymmetric kernel transforms," in *IEEE Conference on Computer Vision and Pattern Recognition (CVPR)*, 2011.

[22] E. Tzeng, J. Hoffman, N. Zhang, K. Saenko, and T. Darrell, "Deep domain confusion: Maximizing for domain invariance," *CoRR*, vol. arXiv:1412.3474, 2014.

[23] M. Long, Y. Cao, J. Wang, and M. I. Jordan, "Learning transferable features with deep adaptation networks," in *International Conference on Machine Learning (ICML)*, 2015.

[24] E. Tzeng, J. Hoffman, T. Darrell, and K. Saenko, "Simultaneous deep transfer across domains and tasks," in *IEEE International Conference on Computer Vision (ICCV)*, 2015, pp. 4068–4076.

[25] Y. Ganin, E. Ustinova, H. Ajakan, P. Germain, H. Larochelle, F. Laviolette, M. Marchand, and V. S. Lempitsky, "Domain-adversarial training of neural networks," *CoRR*, vol. arXiv:1505.07818, 2015.

[26] Y. Ganin and V. Lempitsky, "Unsupervised domain adaptation by back-propagation," in *International Conference on Machine Learning (ICML)*, 2015, pp. 1180–1189.

[27] A. Gretton, A. Smola, J. Huang, M. Schmittfull, K. Borgwardt, and B. Schölkopf, "Covariate shift by kernel mean matching," in *Dataset Shift in Machine Learning*, J. Quiñonero-Candela, M. Sugiyama, A. Schwaighofer, and N. D. Lawrence, Eds. The MIT Press, 2008.

[28] D. Pathak, P. Krahenbuhl, and T. Darrell, "Constrained convolutional neural networks for weakly supervised segmentation," in *Proceedings of the IEEE International Conference on Computer Vision*, 2015, pp. 1796–1804.

[29] H. Noh, S. Hong, and B. Han, "Learning deconvolution network for semantic segmentation," in *IEEE International Conference on Computer Vision (ICCV)*, 2015, pp. 1520–1528.

[30] L.-C. Chen, G. Papandreou, I. Kokkinos, K. Murphy, and A. L. Yuille, "Semantic image segmentation with deep convolutional nets and fully connected crfs," *arXiv preprint arXiv:1412.7062*, 2014.

[31] K. Ganchev, J. Gillenwater, B. Taskar *et al.*, "Posterior regularization for structured latent variable models," *Journal of Machine Learning Research*, vol. 11, no. Jul, pp. 2001–2049, 2010.

[32] Y. Bengio, J. Louradour, R. Collobert, and J. Weston, "Curriculum learning," in *Proceedings of the 26th annual international conference on machine learning*. ACM, 2009, pp. 41–48.

[33] A. Torralba and A. A. Efros, "Unbiased look at dataset bias," in *IEEE Conference on Computer Vision and Pattern Recognition (CVPR)*, 2011.

[34] T. Tommasi, N. Patricia, B. Caputo, and T. Tuytelaars, "A deeper look at dataset bias," *CoRR*, vol. arXiv:1505.01257, 2015.

[35] B. Gong, F. Sha, and K. Grauman, "Overcoming dataset bias: An unsupervised domain adaptation approach," in *NIPS Workshop on Large Scale Visual Recognition and Retrieval (LSVRR)*, 2012.

[36] A. Khosla, T. Zhou, T. Malisiewicz, A. A. Efros, and A. Torralba, "Undoing the damage of dataset bias," in *European Conference on Computer Vision (ECCV)*, 2012, pp. 158–171.

[37] V. M. Patel, R. Gopalan, R. Li, and R. Chellappa, "Visual domain adaptation: A survey of recent advances," *Signal Processing Magazine*, vol. 32, no. 3, pp. 53–69, 2015.

[38] S. J. Pan and Q. Yang, "A survey on transfer learning," *Transactions on Knowledge and Data Engineering*, vol. 22, no. 10, pp. 1345–1359, 2010.

[39] K. Saenko, B. Kulic, M. Fritz, and T. Darrell, "Adapting visual category models to new domains," in *European Conference on Computer Vision (ECCV)*, 2010, pp. 213–226.

[40] K. Bousmalis, N. Silberman, D. Dohan, D. Erhan, and D. Krishnan, "Unsupervised pixel-level domain adaptation with generative adversarial networks," *arXiv preprint arXiv:1612.05424*, 2016.

[41] B. Sun and K. Saenko, "From virtual to reality: Fast adaptation of virtual object detectors to real domains," in *BMVA British Machine Vision Conference (BMVC)*, 2014.

[42] J. Xu, S. Ramos, D. Vazquez, and A. López, "Hierarchical adaptive structural svm for domain adaptation," *CoRR*, vol. arXiv:1408.5400, 2014.

[43] G. Ros, L. Sellart, J. Materzynska, D. Vazquez, and A. M. Lopez, "The synthia dataset: A large collection of synthetic images for semantic segmentation of urban scenes," in *Proceedings of the IEEE Conference on Computer Vision and Pattern Recognition*, 2016, pp. 3234–3243.

[44] D. Vazquez, A. M. López, J. Marín, D. Ponsa, and D. Gerónimo, "Virtual and real world adaptation for pedestrian detection," *Transactions of Pattern Recognition and Machine Analyses (PAMI)*, vol. 36, no. 4, pp. 797 – 809, 2014.

[45] X. Peng and K. Saenko, "Synthetic to real adaptation with deep generative correlation alignment networks," *arXiv preprint arXiv:1701.05524*, 2017.

[46] A. Shrivastava, T. Pfister, O. Tuzel, J. Susskind, W. Wang, and R. Webb, "Learning from simulated and unsupervised images through adversarial training," *arXiv preprint arXiv:1612.07828*, 2016.

[47] J. Shotton, M. Johnson, and R. Cipolla, "Semantic texton forests for image categorization and segmentation," in *2008 IEEE Conference on Computer Vision and Pattern Recognition*, June 2008, pp. 1–8.

[48] J. Tighe and S. Lazebnik, "Superparsing: scalable nonparametric image parsing with superpixels," in *European conference on computer vision*. Springer, 2010, pp. 352–365.

[49] C. Zhang, L. Wang, and R. Yang, "Semantic segmentation of urban scenes using dense depth maps," in *European Conference on Computer Vision*. Springer, 2010, pp. 708–721.

[50] Y. LeCun, L. Bottou, Y. Bengio, and P. Haffner, "Gradient-based learning applied to document recognition," *Proceedings of the IEEE*, vol. 86, no. 11, pp. 2278–2324, 1998.

[51] Z. Wu, C. Shen, and A. v. d. Hengel, "Wider or Deeper: Revisiting the ResNet Model for Visual Recognition," *arXiv preprint arXiv:1611.10080*, 2016.

[52] G. Ros, S. Stent, P. F. Alcantarilla, and T. Watanabe, "Training constrained deconvolutional networks for road scene semantic segmentation," *arXiv preprint arXiv:1604.01545*, 2016.

[53] V. Badrinarayanan, A. Kendall, and R. Cipolla, "Segnet: A deep convolutional encoder-decoder architecture for image segmentation," *arXiv preprint arXiv:1511.00561*, 2015.

[54] H. Zhao, J. Shi, X. Qi, X. Wang, and J. Jia, "Pyramid Scene Parsing Network," *arXiv preprint arXiv:1612.01105*, 2016.

[55] J. Dai, K. He, and J. Sun, "Instance-aware semantic segmentation via multi-task network cascades," in *Proceedings of the IEEE Conference on Computer Vision and Pattern Recognition*, 2016, pp. 3150–3158.

[56] M. Everingham, S. A. Eslami, L. Van Gool, C. K. Williams, J. Winn, and A. Zisserman, "The pascal visual object classes challenge: A retrospective," *International Journal of Computer Vision*, vol. 111, no. 1, pp. 98–136, 2015.

[57] T.-Y. Lin, M. Maire, S. Belongie, J. Hays, P. Perona, D. Ramanan, P. Dollr, and C. L. Zitnick, "Microsoft coco: Common objects in context," in *European Conference on Computer Vision*. Springer, 2014, pp. 740–755.

[58] A. Geiger, P. Lenz, C. Stiller, and R. Urtasun, "Vision meets robotics: The kitti dataset," *The International Journal of Robotics Research*, vol. 32, no. 11, pp. 1231–1237, 2013.

[59] G. Neuhold, T. Ollmann, S. R. Bulo, and P. Kortschieder, "The mapillary vistas dataset for semantic understanding of street scenes," in *Proceedings of the International Conference on Computer Vision (ICCV), Venice, Italy*, 2017, pp. 22–29.

[60] G. J. Brostow, J. Shotton, J. Fauqueur, and R. Cipolla, "Segmentation and recognition using structure from motion point clouds," in *ECCV (1)*, 2008, pp. 44–57.

[61] G. J. Brostow, J. Fauqueur, and R. Cipolla, "Semantic object classes in video: A high-definition ground truth database," *Pattern Recognition Letters*, vol. 30, no. 2, pp. 88–97, 2009.

[62] S. Hong, J. Oh, H. Lee, and B. Han, "Learning transferrable knowledge for semantic segmentation with deep convolutional neural network," in *Proceedings of the IEEE Conference on Computer Vision and Pattern Recognition*, 2016, pp. 3204–3212.

[63] G. Papandreou, L.-C. Chen, K. P. Murphy, and A. L. Yuille, "Weakly- and semi-supervised learning of a deep convolutional network for semantic image segmentation," in *Proceedings of the IEEE International Conference on Computer Vision*, 2015, pp. 1742–1750.

[64] P. O. Pinheiro and R. Collobert, "From image-level to pixel-level labeling with convolutional networks," in *Proceedings of the IEEE Conference on Computer Vision and Pattern Recognition*, 2015, pp. 1713–1721.

[65] A. Gaidon, Q. Wang, Y. Cabon, and E. Vig, "Virtual worlds as proxy for multi-object tracking analysis," in *Proceedings of the IEEE Conference on Computer Vision and Pattern Recognition*, 2016, pp. 4340–4349.

[66] A. Geiger, P. Lenz, C. Stiller, and R. Urtasun, "Vision meets robotics: The kitti dataset," *International Journal of Robotics Research (IJRR)*, 2013.

[67] A. Shafaei, J. J. Little, and M. Schmidt, "Play and learn: using video Games to train computer vision models," *arXiv preprint arXiv:1608.01745*, 2016.

[68] S. Sankaranarayanan, Y. Balaji, A. Jain, S. N. Lim, and R. Chellappa, "Unsupervised domain adaptation for semantic segmentation with gans," *arXiv preprint arXiv:1711.06969*, 2017.

[69] K. Saito, K. Watanabe, Y. Ushiku, and T. Harada, "Maximum classifier discrepancy for unsupervised domain adaptation," *arXiv preprint arXiv:1712.02560*, 2017.

[70] Y. Chen, W. Li, and L. Van Gool, "Road: Reality oriented adaptation for semantic segmentation of urban scenes," *arXiv preprint arXiv:1711.11556*, 2017.

[71] Z. Wu, X. Han, Y.-L. Lin, M. G. Uzunbas, T. Goldstein, S. N. Lim, and L. S. Davis, "Dcan: Dual channel-wise alignment networks for unsupervised scene adaptation," *arXiv preprint arXiv:1804.05827*, 2018.

[72] Y. Ganin and V. Lempitsky, "Unsupervised domain adaptation by back-propagation," *arXiv preprint arXiv:1409.7495*, 2014.

[73] E. Kolve, R. Mottaghi, D. Gordon, Y. Zhu, A. Gupta, and A. Farhadi, "Ai2-thor: An interactive 3d environment for visual ai," *arXiv preprint arXiv:1712.05474*, 2017.

[74] C. Bucilu, R. Caruana, and A. Niculescu-Mizil, "Model compression," in *Proceedings of the 12th ACM SIGKDD international conference on Knowledge discovery and data mining*. ACM, 2006, pp. 535–541.

[75] G. Hinton, O. Vinyals, and J. Dean, "Distilling the knowledge in a neural network," *arXiv preprint arXiv:1503.02531*, 2015.

[76] H. Bilen, M. Pedersoli, and T. Tuytelaars, "Weakly supervised object detection with posterior regularization," in *BMVA British Machine Vision Conference (BMVC)*, 2014.

[77] Z. Hu, X. Ma, Z. Liu, E. Hovy, and E. Xing, "Harnessing deep neural networks with logic rules," *arXiv preprint arXiv:1603.06318*, 2016.

[78] C. Szegedy, S. Ioffe, V. Vanhoucke, and A. Alemi, "Inception-v4, inception-resnet and the impact of residual connections on learning," *arXiv preprint arXiv:1602.07261*, 2016.

[79] Z. Li and J. Chen, "Superpixel segmentation using linear spectral clustering," in *Proceedings of the IEEE Conference on Computer Vision and Pattern Recognition*, 2015, pp. 1356–1363.

[80] R. Mottaghi, X. Chen, X. Liu, N.-G. Cho, S.-W. Lee, S. Fidler, R. Urtasun, and A. Yuille, "The role of context for object detection and semantic segmentation in the wild," in *IEEE Conference on Computer Vision and Pattern Recognition (CVPR)*, 2014, pp. 891–898.

[81] D. H. Foster, "Color constancy," *Vision research*, vol. 51, no. 7, pp. 674–700, 2011.

[82] C. Barata, M. E. Celebi, and J. S. Marques, "Improving dermoscopy image classification using color constancy," *IEEE journal of biomedical and health informatics*, vol. 19, no. 3, pp. 1146–1152, 2015.

[83] A. Gijsenij, T. Gevers, and J. Van De Weijer, "Computational color constancy: Survey and experiments," *IEEE Transactions on Image Processing*, vol. 20, no. 9, pp. 2475–2489, 2011.

[84] —, "Generalized gamut mapping using image derivative structures for color constancy," *International Journal of Computer Vision*, vol. 86, no. 2, pp. 127–139, 2010.

[85] K. Simonyan and A. Zisserman, "Very deep convolutional networks for large-scale image recognition," *CoRR*, vol. arXiv:1409.1556, 2014.

[86] M. D. Zeiler, "ADADELTA: an adaptive learning rate method," *arXiv preprint arXiv:1212.5701*, 2012.

[87] F. Chollet, "keras," <https://github.com/fchollet/keras>, 2015.

[88] R. Al-Rfou, G. Alain, A. Almahairi, C. Angermueller, D. Bahdanau, N. Ballas, F. Bastien, J. Bayer, A. Belikov, A. Belopolsky, and others, "Theano: A Python framework for fast computation of mathematical expressions," *arXiv preprint arXiv:1605.02688*, 2016.

[89] Z. Wu, C. Shen, and A. v. d. Hengel, "Wider or deeper: Revisiting the resnet model for visual recognition," *arXiv preprint arXiv:1611.10080*, 2016.

[90] A. Gretton, K. M. Borgwardt, M. J. Rasch, B. Schölkopf, and A. Smola, "A kernel two-sample test," *Journal of Machine Learning Research*, vol. 13, no. Mar, pp. 723–773, 2012.

[91] D. G. Lowe, "Distinctive image features from scale-invariant keypoints," *International journal of computer vision*, vol. 60, no. 2, pp. 91–110, 2004.

[92] F. Perronnin, J. Sánchez, and T. Mensink, "Improving the fisher kernel for large-scale image classification," *Computer Vision–ECCV 2010*, pp. 143–156, 2010.

[93] F. Perronnin and C. Dance, "Fisher kernels on visual vocabularies for image categorization," in *IEEE Conference on Computer Vision and Pattern Recognition (CVPR)*. IEEE, 2007, pp. 1–8.

[94] J.-Y. Zhu, T. Park, P. Isola, and A. A. Efros, "Unpaired image-to-image translation using cycle-consistent adversarial networks," in *Proceedings of the IEEE Conference on Computer Vision and Pattern Recognition*, 2017, pp. 2223–2232.

[95] F. Yu, V. Koltun, and T. Funkhouser, "Dilated residual networks," in *Computer Vision and Pattern Recognition (CVPR)*, 2017.

[96] A. Ruano, "Deepgtav," <https://github.com/aitorzip/DeepGTAV>, 2017.